LA-UR- 99-1223

Approved for public release; distribution is unlimited.

RECEIVED
SEP 01 1999
OSTI

Title: DISCONTINUOUS FINITE ELEMENT SN METHODS ON 3-D UNSTRUCTURED GRIDS

Author(s): T.A.Wareing
J.M. McGhee
J.E. Morel
S.D. Pautz

Submitted to: Mathematics & Computation, September 27-30, 1999, Madrid, Spain

Los Alamos
NATIONAL LABORATORY

Los Alamos National Laboratory, an affirmative action/equal opportunity employer, is operated by the University of California for the U.S. Department of Energy under contract W-7405-ENG-36. By acceptance of this article, the publisher recognizes that the U.S. Government retains a nonexclusive, royalty-free license to publish or reproduce the published form of this contribution, or to allow others to do so, for U.S. Government purposes. Los Alamos National Laboratory requests that the publisher identify this article as work performed under the auspices of the U.S. Department of Energy. Los Alamos National Laboratory strongly supports academic freedom and a researcher's right to publish; as an institution, however, the Laboratory does not endorse the viewpoint of a publication or guarantee its technical correctness.

DISCLAIMER

This report was prepared as an account of work sponsored by an agency of the United States Government. Neither the United States Government nor any agency thereof, nor any of their employees, make any warranty, express or implied, or assumes any legal liability or responsibility for the accuracy, completeness, or usefulness of any information, apparatus, product, or process disclosed, or represents that its use would not infringe privately owned rights. Reference herein to any specific commercial product, process, or service by trade name, trademark, manufacturer, or otherwise does not necessarily constitute or imply its endorsement, recommendation, or favoring by the United States Government or any agency thereof. The views and opinions of authors expressed herein do not necessarily state or reflect those of the United States Government or any agency thereof.

DISCLAIMER

Portions of this document may be illegible in electronic image products. Images are produced from the best available original document.

Discontinuous Finite Element S_N Methods on 3-D Unstructured Grids

T. A. Wareing, J. M. McGhee, J. E. Morel and S. D. Pautz
Los Alamos National Laboratory
Transport Methods Group
Los Alamos, NM 87545
wareing@lanl.gov mcghee@lanl.gov jim@lanl.gov pautz@lanl.gov

Abstract

Discontinuous finite element methods for the S_N equations on 3-D unstructured tetrahedral and hexahedral meshes are presented. Solution techniques including Source Iteration and diffusion-synthetic acceleration are described. Numerical results are presented which demonstrate the accuracy and efficiency of these methods.

1 Introduction

The purpose of this paper is to present methods for solving the S_N equations on 3-D unstructured tetrahedral and hexahedral meshes using the discontinuous finite-element method (DFEM) for the spatial discretization. The majority of DFEMs developed within the reactor physics community have been rectangular-mesh methods. Notable exceptions are the methods used in the TRIPLET (Reed, 1973), TRIDENT (Seed, 1977), and ZEPHYR (Mordant, 1981) discrete ordinates codes. TRIPLET and TRIDENT are 2-D triangular-mesh codes. Their meshes are actually semi-structured rather than fully structured because the triangles are located on bands. The ZEPHYR code has a fully unstructured mesh consisting of arbitrary combinations of quadrilaterals and triangles. There are two significant complications encountered when applying DFEMs to the S_N equations on 2-D unstructured meshes that are not encountered when applying them on 2-D rectangular meshes:

> The finite-element matrix elements must be evaluated by quadrature because they cannot be analytically integrated.
>
> The lower-triangular ordering of the angular flux unknowns required to solve the source iteration equations via the back-substitution or sweeping technique is mesh-dependent. Thus this ordering must be explicitly determined for each direction via a computational algorithm. On rectangular meshes, this ordering depends upon direction, but it is mesh-independent and trivial to recognize. It has been observed that a lower-triangular ordering exists on all 2-D unstructured meshes as long as the mesh is non-re-entrant as a whole, and each element (spatial cell) within the mesh is non-re-entrant.

Further complications are encountered when DFEMS are applied on 3-D unstructured meshes:

> Because the faces of general hexahedra can be non-planar, a given direction can be incident on one part of a element face and exiting on the other part. This causes the finite-element definition of the angular flux to change on the interior of element faces, whereas such changes never occur with flat faces. These face-interior changes require separate matrix-element integrations within the incident and exiting regions of the face because each region has a different basis function representation for the flux. Since standard finite-element quadratures are intended to integrate

a single flux representation over a whole face, they can be very inaccurate for performing these double-representation integrations. Furthermore, having directions that are both incident and exiting on the same face make a lower-triangular ordering impossible because the two elements sharing that face become mutually-dependent.

We initially assumed that if a 3-D unstructured mesh were non-re-entrant as a whole, and if all of the elements in the mesh were non-re-entrant and had flat faces, a lower-triangular ordering of the angular flux unknowns would exist. However, we found that this is not necessarily true. It is possible for "rings" of mutual dependency to form on 3-D unstructured meshes even if the previously described mesh criteria are met. When this occurs, a lower-triangular ordering of the angular flux unknowns does not exist.

Thus, if one is develop a DFEM S_N method for 3-D unstructured meshes, one must deal with the complications described above. Our strategy for dealing with them relies on the fact that these complications will rarely occur on well-shaped, i.e. not highly skewed, meshes. The full details are given later, but a high-level description of our strategy can be given as follows:
We deal with a directions that is both incident and exiting on the same face by defining the direction to be either incident or exiting over the whole face via a single average face normal. The finite-element flux representation is then uniquely defined over the entire face. Furthermore, this solves the local problem of mutual coupling between the elements that share the face, but global dependency rings can still form. We use graph theory to identify mutually-dependent rings of elements in the sweep ordering process. The mutual dependence is effectively broken by assuming that the incoming fluxes for one element in the ring are known. This allows one to continue the ordering process even though the resulting system of source iteration equations is not lower triangular. Because the equations are not lower triangular, an exact solution is not obtained after each sweep is performed. Fortunately, our computational testing indicates that the occurrence of mutually-dependent rings is sufficiently rare that they have a negligible effect on the convergence rate of the source iteration process.
The remainder of this paper is organized as follows: in Section 2, we describe the DFEM spatial differencing of the S_N equations on 3-D unstructured meshes; in Section 3, we describe the solution method for solving these DFEM S_N equations; in Section 4, we present some numerical results; and in Section 5 we end with some conclusions.

2 DFEM Spatial Differencing

To simplify our description of the DFEM spatial differencing, we only consider the single energy group S_N equations with isotropic scattering, although this is not a restriction. The S_N equations for volume V with boundary δV are given by

$$\hat{\Omega}_m \cdot \vec{\nabla} \Psi_m(\vec{r}) + \sigma_t(\vec{r})\Psi_m(\vec{r}) = \sigma_t(\vec{r})\Phi(\vec{r}) + q_m(\vec{r}), \tag{1}$$

plus boundary conditions. Here standard notation is used. Expanding the $\vec{\nabla}$ operator and $\hat{\Omega}$ using the standard summation convention (i.e. a repeated index in the same multiplicative term implies a summation) and suppressing the m subscripts, Eq.(1) becomes

$$\hat{\Omega}_i \frac{\partial}{\partial r_i}\Psi(r) + \sigma_t(r)\Psi(r) = \sigma_s(r)\Phi(r) + q(r), \tag{2}$$

where the individual components of $\hat{\Omega}$ have been written as $\hat{\Omega}_i$ and the individual components of $\vec{\nabla}$ have been written as $\partial/\partial r_i$, where $r_1 = x$, $r_2 = y$ and $r_3 = z$. The indices run from one to the

number of spatial dimensions. Unless otherwise noted, this summation convention will be used in all the equations that follow.

We begin the development by assuming that the problem domain has been divided into a unstructured spatial grid of volume elements. The element shapes are unspecified for now, but we do require that the vertexes be connected by straight lines. The material properties within each spatial element are assumed to be constant. The DFEM derivation begins by considering element, k, with volume V_k and surface δV_k. We define approximate angular and scalar flux functions within element k:

$$\Psi(r) \cong \overrightarrow{\Theta}^T \overrightarrow{\psi}, \tag{3}$$

$$\Phi(r) \cong \overrightarrow{\Theta}^T \overrightarrow{\phi}, \tag{4}$$

where $\overrightarrow{\Theta}^T$ is the transpose of a column vector of spatial interpolation (basis) functions. The basis functions are chosen to give appropriate nodal displacements when the coordinates of corresponding nodes are inserted into Eqs. (3) and (4). Therefore, $\overrightarrow{\psi}$ and $\overrightarrow{\phi}$ are column vectors of nodal angular and scalar fluxes. Next, we apply the Galerkin method, which consists of multiplying Eq. (2) by $\overrightarrow{\Theta}$, integrating over V_k, and inserting Eqs. (3)-(4) into the resulting equations. This operation guarantees the orthogonality of the residuals to the space spanned by the spatial basis functions, thus minimizing, in a certain sense, the error introduced by the approximation introduced in Eq. (3). Carrying out this operation and using the divergence theorem, we obtain:

$$\int_{\delta V_k} \hat{\Omega}_i \hat{n}_i \overrightarrow{\Theta}\, \overrightarrow{\Theta}^T \overrightarrow{\psi}^s d\delta V - \int_{V_k} \hat{\Omega}_i \frac{\partial \overrightarrow{\Theta}}{\partial r_i} \overrightarrow{\Theta}^T \overrightarrow{\psi} dV + \int_{V_k} \overrightarrow{\Theta} \left\{ \sigma_t \overrightarrow{\Theta}^T \overrightarrow{\psi} - \sigma_s \overrightarrow{\Theta}^T \overrightarrow{\phi} - q(r) \right\} dV = 0. \tag{5}$$

Here, $\hat{n}_i$ is the i-th component of the outward directed unit normal vector, $\hat{n}$, to δV_k and $\overrightarrow{\psi}^s$ is the column vector of boundary nodal angular fluxs. For each element,

$$\delta V_k = \sum_{l=l}^{N_{faces}} \delta V_{k,l}, \tag{6}$$

where l represents the face number and N_{faces} is the total number of faces enclosing element k, where $N_{faces} = 4$ for tetrahedral elements and $N_{faces} = 6$ for hexahedral elements. To complete the derivation we need to define the element boundary angular fluxes. This discontinuous representation for $\overrightarrow{\psi}^s$ on each face of the element is given by

$$\overrightarrow{\psi}^s = \begin{array}{ll} \overrightarrow{\psi}, & \hat{\Omega}_i \hat{n}_i^{av} > 0 \\ \overrightarrow{\psi}^{inc}, & \hat{\Omega}_i \hat{n}_i^{av} < 0 \end{array}. \tag{7}$$

Here, $\overrightarrow{\psi}^{inc}$ is the corresponding column vector of nodal angular flux values of the element that shares the same face as element k and $\hat{n}^{av}$ is the average outward directed unit normal vector of the face.

Equation (7) requires some explanation. For elements with planar faces (tetrahedra) these definitions are consistent with the finite-element formalism. For non-planar faces, the unit normal vector to the face is not constant across the face and a given direction can be both incident and exiting to the face. This results in a mutual dependency between the elements that share the face and thereby makes a lower triangular ordering impossible. If the unit normal vector to a face does not change sign then

the use of an average normal for defining incident and exiting fluxes remains fully consistent with the finite-element formalism. If the unit normal vector to a face does change sign we define each given direction to either be incident or exiting across the entire face based upon the average outward directed unit normal vector to the face. This is not consistent with the finite-element formalism and therefore represents an additional approximation.

3 Solution Technique

The DFEM equations are solved using source iteration (SI) in conjunction with diffusion-synthetic acceleration (DSA), as described by the following equations:

$$\hat{\Omega} \cdot \vec{\nabla} \Psi^{(\ell+1/2)} + \sigma_t(r)\Psi^{(\ell+1/2)} = \sigma_s \Phi^{(\ell)} + Q, \tag{8}$$

$$-\vec{\nabla} \cdot \frac{1}{3\sigma_t} \vec{\nabla} \delta\Phi^{(\ell+1)} + \sigma_a(r)\delta\Phi^{(\ell+1)} = \sigma_s(r)\left(\Phi^{(\ell+1/2)} - \Phi^{(\ell+1)}\right), \tag{9}$$

$$\Phi^{(\ell+1)} = \Phi^{(\ell+1/2)} + \delta\Phi^{(\ell+1)}. \tag{10}$$

Here, ℓ is the iteration index.Equation (9) is the sweep equation and Eq. (9) is the DSA equation.

3.1 Source Iteration and Transport Sweeps

The discretization of Eq. (8) in angle and space yields, for each angle in the discrete set, a system of equations whose associated matrix can be written in block lower triangular form (the sweep matrix), where each block is usually associated with the unknowns in a single spatial element. The dependencies between the elements for any angle can also be expressed in terms of a directed graph. If this sweep graph is acyclic, then each of the blocks in the matrix is associated with a single element; if the graph is cyclic then at least one of the blocks is associated with more than one element. This means that the source iteration equations can no longer be exactly solved using a sweep.
Each system of DFEM S_N equations is solved by the method of sweeping. The spatial elements are placed into an ordered list in which the order results in a block lower triangular matrix. Each block is solved in succession. Physically this solution order resembles a wave front propagating through the mesh roughly in the direction of the associated angle. In the case of a cyclic sweep graph a depth first search algorithm (Aho, et al., 1974) is used to determine the identities of the elements in each cycle (associated with a large block in the matrix). These cycles are "broken open" by approximating one or more unknown incoming face fluxes with the values from the previous source iteration; this approximation yields a modified sweep matrix in which each block refers to the unknowns of only one element.
Although most of the meshes we have generated and examined have yielded only directed acyclic sweep graphs, we have observed cyclic graphs in both tetrahedral and hexahedral meshes. The extra effort needed to break open the cycles has not resulted in any appreciable increase in run time, nor has the use of previous iterate information noticeably degraded the performance or stability of the source iteration technique or DSA method.

3.2 Acceleration Equations

Specific details of DSA are widely available in the literature (Alcouffe, 1977) and (Larsen, 1982). One very important and well known fact about DSA is that the discretization of Eq.(9) must be consistent (or nearly consistent) with the discretization of Eq. (8). The four-step method of (Larsen,

1982) is one way to obtain completely consistent differencing of Eq.(9) for all differencing schemes, but for advanced differencing schemes such as DFEMs in multidimensions, the resulting P_1 system of equations cannot be collapsed into a single discretized diffusion equation. Adams and Martin have proposed a "modified four-step" DSA method (Adams and Martin, 1992) for DFEMs, where the diffusion differencing is obtained by applying a DFEM method to the diffusion equation. Their method leads to a single discretized diffusion equation, which is both non-standard and non-symmetric . Both the four-step and modified four-step methods are stable and effective for DFEMs, but the resulting equations are difficult to solve in an efficient manner, except for certain simple mesh configurations. Wareing, Larsen and Adams (Wareing, et al., 1991) have developed yet another approach for obtaining nearly consistent DSA equations for DFEMs. This approach leads to a discretized diffusion equation that can be solved very efficiently, however, although the method is always stable, the effectiveness is significantly degraded for skewed (high aspect ratio) elements. We have chosen an adaptation of theWareing, Larsen and Adams method.

The discretization of Eq. (9), using an adaptation of the Wareing, Larsen and Adams method, replaces the DFEM DSA equation with continuous finite element (CFEM) DSA equation. In addition, a local within-element mapping procedure is used to project from the CFEM scalar flux corrections to the approximated DFEM scalar flux corrections. This mapping is derived from the Adams and Martin DFEM DSA equations. The CFEM discretization is given by

$$\sum_{k=1}^{N_{element}} \left\{ -\frac{1}{3\sigma_t} \int_{\delta V_k} n_i \vec{\Theta} \frac{\partial \vec{\Theta}^T}{\partial r_i} \vec{\delta\phi}_{cont}^{(\ell+1)} d\delta V + \frac{1}{3\sigma_t} \int_{V_k} \left(\frac{\partial \vec{\Theta}}{\partial r_i} \right) \left(\frac{\partial \vec{\Theta}^T}{\partial r_j} \right) \vec{\delta\phi}_{cont}^{(\ell+1)} dV \right.$$

$$\left. + \sigma_a \int_{V_k} \vec{\Theta}\, \vec{\Theta}^T \vec{\delta\phi}_{cont}^{(\ell+1)} dV = \sigma_s \int_{V_k} \vec{\Theta}\, \vec{\Theta}^T \left(\vec{\phi}_{disc}^{(\ell+1/2)} - \vec{\phi}_{disc}^{(\ell)} \right) dV \right\}, \tag{11}$$

with Marshak boundary conditions, which leads to a N_{vertex} x N_{vertex} symmetric positive-definite matrix, where N_{vertex} and $N_{element}$ is the number of vertices and elements in the mesh, respectively. The local within-element mapping is given by the following:

$$\frac{1}{2} \int_{\delta V_k} \vec{\Theta}\, \vec{\Theta}^T \vec{\delta\phi}_{disc}^{(\ell+1)} d\delta V + \sigma_a \int_{V_k} \vec{\Theta}\, \vec{\Theta}^T \vec{\delta\phi}_{disc}^{(\ell+1)}$$

$$= \frac{1}{2} \int_{\delta V_k} \vec{\Theta}\, \vec{\Theta}^T \vec{\delta\phi}_{cont}^{(\ell+1)} d\delta V + \sigma_s \int_{V_k} \vec{\Theta}\, \vec{\Theta}^T \left(\vec{\phi}_{disc}^{(\ell+1/2)} - \vec{\phi}_{disc}^{(\ell)} \right) dV. \tag{12}$$

4 Numerical Results

4.1 Test Problem One

The first test problem is designed to compare the accuracy of the DFEM on unstructured hexahedral and tetrahedral meshes. It consists of a 1-D homogeneous slab of isotropically-scattering material with a total length of 1 *cm*, a total cross section of 2 cm^{-1}, a scattering ratio of 0.5, a spatially-constant isotropic homogeneous source of 1 $\frac{particle}{cm^3-s}$, and vacuum boundaries each boundary. An analytic S_2(or diffusion with Mark boundary conditions) to the test problem is straightforward to obtain. In particular, the scalar flux solution is given by

$$\phi = 1 - \frac{\exp\left[\sqrt{6}\,(1-x)\right] + \exp\left[\sqrt{6}x\right]}{1 - \frac{1}{\sqrt{2}} + \exp\left[1 + \frac{1}{\sqrt{2}}\right]}.$$

The problem is modeled in 3-D with reflecting boundaries on each boundary perpendicular to the y and z axes. Calculations were performed on a sequence of four tetrahedral grids, four orthogonal hexahedral grids and four non-orthogonal hexahedral grids.. The four tetrahedra meshes, as described in Table (1), are unstructured but similar in all respects other than number and size of the tetrahedral elements. The four orthogonal and non-orthogonal hexahedral mesh sequences use 5, 10, 20 and 40 elements per side of a 1 cm single material cube. The non-orthogonal meshes begin with the orthogonal mesh, but the widths are perturbed using pseudo-random numbers. In particular, each vertex (except the first and last) was given a perturbed coordinate as follows:

$$z_p = z_u + 0.15\Delta x_u(2R_a - 1) \ ,$$

where $z_p$denotes the unperturbed element width, $z_u$denotes the unperturbed coordinate, Δx_udenotes the unperturbed element width, and R_a denotes a pseudo-random number. The element edge widths were perturbed to ensure elimination of anomalous accuracy effects that are sometime observed with perfectly uniform meshes. The average element edge width is approximately the same as that for the orthogonal mesh.

Table 1: Tetrahedral Mesh Description for Test Problem One.

Mesh ID	Tetrahedra	Average Cell Edge Width (mfp)
1	192	0.7070
2	1536	0.3536
3	12228	0.1770
4	98304	0.0884

The absolute relative error in the total absorption rate as a function of average element edge width is plotted in Figure (1) for the tetrahedral grid, orthogonal hexahedral grid and non-orthogonal hexahedral grid S_2 solutions. All of the solutions exhibit third-order accuracy. The most accurate solution comes from using the tetrahedral grid. The orthogonal and non-orthogonal hexahedral grid solutions show comparable accuracy with the non-orthogonal hexahedral grid being slightly less accurate (which cannot be seen in the figure).

4.2 Test Problem Two

The second test problem is designed to show the effectiveness of the DSA method with tetrahedral meshes and non-orthogonal hexahedral meshes with and without degenerate elements. A degenerate element is formed when one or more verticies have the same coordinates. The problem consists of a homogeneous sphere with vacuum boundary conditions. We vary the total cross section and the scattering ratio. The tetrahedral mesh consists of 607 tetrahedra with an average element edge width of 0.259 cm. The hexahedral mesh without degeneracies is consists of 648 hexahedra with an average element edge width of 0.317 cm. The hexahedral mesh with degeneraces (some of the hexahedra have degenerated into tetrahedra, wedges and pyramids) consists of 576 hexahedra and the average element edge width is unknown.
The spectral radii for each mesh as a function of total cross section and scattering ratio is given in Tables (2),(3) and (4) for the tetrahedral mesh , hexahedral mesh without degeneracies and hexahedral mesh with degenercies respectively. The spectral radii for a small total cross section are small because of the large amount of leakage.

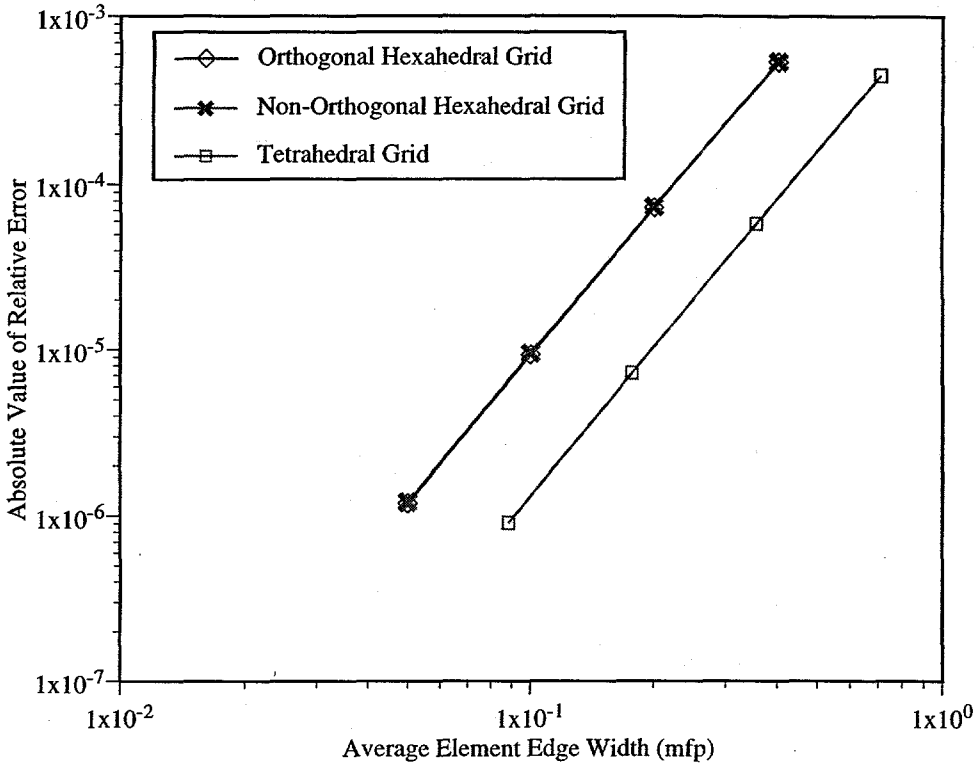

Figure 1: Absolute Error in Absorption Rate for Test Problem One.

Table 2: Spectral Radius for Test Problem Two Using Tetrahedral Mesh.

σ_t	$c = 1.00$	$c = 0.99$	$c = 0.90$
0.1	0.03	0.03	0.03
1.0	0.17	0.17	0.15
10.0	0.58	0.57	0.49
100.0	0.90	0.87	0.61
1000.0	0.95	0.71	0.25

Here we see that the DSA method is very effective under most conditions. For the tetrahedral mesh and hexahedral mesh without degeneracies, we see that the spectral radii degrades as $c \rightarrow 1$ and as σ_t becomes large. Clearly this effect is more pronounced for the hexadedral mesh with degeneracies. With increasing amounts of absorption, this degredation in the spectral radii diminishes. These results demonstrate that the DSA method should be very effective for most neutronic problems provides the elements are not too skewed, but may be inadequate for radiative transfer problems.

4.3 Test Problem Three

This problem is designed to show the efficiency of the DSA method on a heterogeneous test problem. The problem is a sphere with a diameter of 2.0 cm containing a 1.0 cm x 1.0 cm x 1.0 cm cube in the center. The sphere has a total cross section in of 10 $cm^{-1}$and the scattering ratio is unity. The total cross section in the box, $\sigma_{t,box}$, is set to $0.01 cm^{-1}$,$1.0\ cm^{-1}$ or $10.0\ cm^{-1}$ and the scattering ratio is 0.9. There is a homogeneous source of strength 1 $\frac{particle}{cm^3-s}$ inside the box. The problem with two meshes,

Table 3: Spectral Radius for Test Problem Two Using Hexahedral Mesh Without Degenerate Elements.

σ_t	$c = 1.00$	$c = 0.99$	$c = 0.90$
0.1	0.03	0.03	0.03
1.0	0.17	0.17	0.15
10.0	0.36	0.36	0.32
100.0	0.68	0.64	0.54
1000.0	0.86	0.72	0.35

Table 4: Spectral Radius for Test Problem Two Using Hexahedral Mesh With Degenerate Elements.

σ_t	$c = 1.00$	$c = 0.99$	$c = 0.90$
0.1	0.05	0.05	0.05
1.0	0.27	0.27	0.23
10.0	0.75	0.74	0.63
100.0	1.00	0.99	0.87
1000.0	1.00	0.99	0.71

an unstructured tetrahedral mesh and a hexahedral mesh without degeneracies. The tetrahedral mesh contains 1735 elements and is shown if Figure (2). The hexahedral mesh contains 2016 elements and is shown in Figure (3). The problem was solved with S_4 level-symmetric quadrature with a convergence criterion of 10^{-4}.

Table (5) and (6) give the SI and DSA CPU time and number of transport iterations for the tetrahedral and hexahedral meshes, respectively. The absortion rate percentage is given to verify that the two element mesh types are giving the same answer. Here we see that the DSA method is very effective and efficient for this problem. The DSA method is very efficient and only increase the time per iteration by about 5 % for the tetrahedral mesh and by about 6 % for the hexahedral mesh.

Table 5: Tetrahedral Mesh CPU time and Iteration Counts for Test Problem Three.

	SI		DSA		
$\sigma_{t,box}$	CPU Time	Iterations	CPU Time	Iterations	Absorption Rate (%)
0.1	573.8	157	57.9	15	1.276
1.0	558.0	153	45.8	12	11.78
10.0	496.7	136	35.0	9	62.10

5 Conclusions

We have successfully developed and implimented discontinuous finite element methods for the S_N equations on 3-D unstructured tetrahedral and hexahedral grids. We have demonstrated that the methods are third order accurate even on non-orthogonal meshes. The source iterations have successfully been accelerated with a DSA method that is efficient and effective for most types of problems, especially neutronics problems. We are presently investigating other DSA techniques that are effective for all types of problems, especially thermal radiative transfer problems.

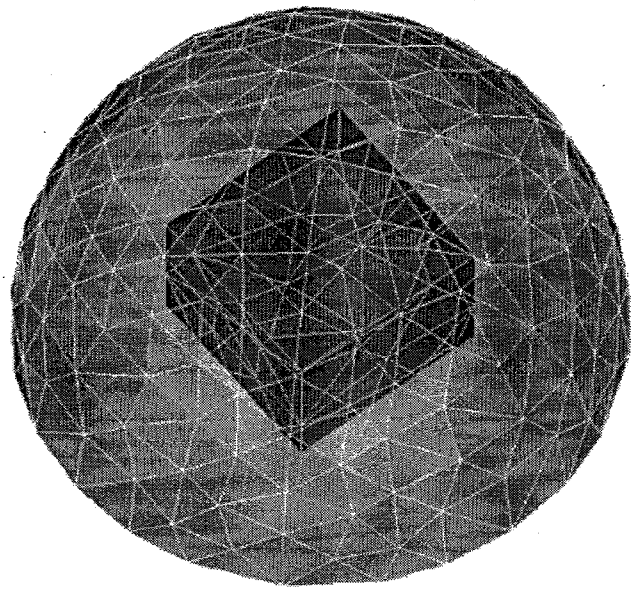

Figure 2: Tetrahedral Mesh For Test Problem Three.

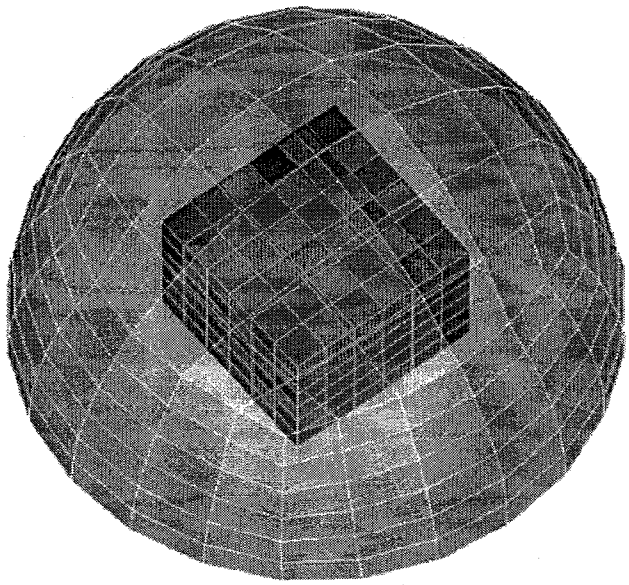

Figure 3: Hexahedral Mesh For Test Problem Three.

Table 6: Hexahedral Mesh CPU time and Iteration Counts for Test Problem Three.

	SI		DSA		
$\sigma_{t,box}$	CPU Time	Iterations	CPU Time	Iterations	Absorption Rate (%)
0.1	1863.8	157	118.1	9	1.277
1.0	1822.5	153	105.0	8	11.79
10.0	1619.3	137	79.7	6	62.17

Acknowledgments

This work was performed under the auspices of the United States Department of Energy.

References

[Reed, 1973] Reed, W. H. et al., TRIPLET: A Two-Dimensional, Multigroup, Triangular-Mesh, Planar Geometry, Explicit Transport Code. Los Alamos Scientific Laboratory Report LA-5428-MS, (1973).

[Seed, 1977] Seed, T. J. et al., TRIDENT: A Two-Dimensional, Multigroup, Triangular-Mesh, Planar Geometry, Explicit Transport Code. Los Alamos Scientific Laboratory Report LA-6735-MS, (1977).

[Mordant, 1981] Mordant, M., Some Efficient Lagrangian Mesh Finite Elements Encoded in ZEPHYR for Two Dimensional Transport Calculations. Annals of Nuclear Energy, 18, 609 (1981).

[Aho, et al., 1974] Aho, A.V, Hopcroft, J.E. and Ullman, J.D., The Design and Analysis of Computer Algorithms. Addison-Wesley, Reading, MA (1974).

[Alcouffe, 1977] Alcouffe, R.E. Diffusion Synthetic Acceleration Methods for the Diamond Differenced Discrete Ordinate Equations. Nucl. Sci. Eng., 66, 344 ((1977).

[Larsen, 1982] Larsen, E.W. Unconditionally Stable Diffusion Synthetic Acceleration Methods for the Slab Geometry Discrete Ordinates Equations Part1: Theory. Nucl. Sci. Eng., 82, 47 (1982).

[Adams and Martin, 1992] Adams, M.L. and Martin, W.R. Diffusion Synthetic Acceleration of Discontinuous Finite Element Transport Iterations. Nucl. Sci. Eng., 111, 145 (1992).

[Wareing, et al, 1991] Wareing, T.A., Larsen, E.W. and Adams, M.L., Diffusion Accelerated Discontinuous Finite Element Schemes for the S_N Equations in Slab and X-Y Geometries. Proc. Int. Topl. Mtg on Advances in Mathematics, Computations and Reactor Physics, Pittsburg, PA., USA, April 29 - May 2, 1991, American Nuclear Society (1991).